 FDMP, vol.9, no.3, pp.209-234, 2013

Comparison and a Possible Source of Disagreement between Experimental and Numerical Results in a Czochralski Model

V. Haslavsky, E. Miroshnichenko, E. Kit, and A. Yu. Gelfgat

Abstract: Experimental and numerical observations of oscillatory instability of melt flow in a Czochralski model are compared, and a disagreement observed at small crystal dummy rotation rates is addressed. To exclude uncertainties connected with flow along the free surface, the latter is covered by a no-slip thermally insulating ring. Experiments reveal an appearance of oscillations at temperature differences smaller than the numerically predicted critical ones. At the same time, a steep increase of the oscillations amplitude is observed just beyond the computed threshold values. By increasing the dummy rotation gradually, we are able to qualitatively confirm the numerically predicted flow destabilization. A good quantitative comparison is reached only with a rather strong rotation of the crystal dummy. Focusing on the disagreement in the non-rotating case, we argue that the experimentally observed instability is triggered by an external excitation that results from low-amplitude temperature oscillations in thermostatic baths. This argument is supported by a numerical simulation of the parametrically excited model.

Keywords: Czochralski growth, oscillatory instability, convection, rotating flows.

1 Introduction

Czochralski melt flow is one of the challenging fluid flow / heat transfer problems related to non-isothermal flow driven by buoyancy, thermocapillarity and rotation [Hurle (1983); Jones (1983); Jones (1989); Ristorcelli and Lumley (1992)]. The problem directly relates to the Czochralski crystal growth process, which is used for production of most of the bulk monocrystals [Hurle and Cockayne (1994); Müller (2007)]. Among others, one of the problems of the Czochralski flow laboratory and numerical modeling is prediction of steady-oscillatory transition, which takes place at certain values of the governing parameters, and directly affects the quality of the growing crystals [Hurle (1983); Kakimoto (1995); Müller (2007)]. In large Prandtl number melts, $Pr>1$, the instabilities appear as spoke patterns, cold plumes

and oscillating jets [Jones (1983); Munakata and Tanasawa (1990); Hintz, Schwabe and Wilke (2001); Hintz and Schwabe (2001); Schwabe (2002); Teitel, Schwabe and Gelfgat (2008)]. These instabilities are studied and qualitatively described as a result of the Rayleigh-Bénard mechanism that can be localized in different flow areas and, therefore, results in different patterns [Gelfgat, Bar-Yoseph, Solan and Kowalewski (1999); Gelfgat (2011)].

In the course of study of melt flows in the Czochralski crystal growth configuration, many model experiments were performed (e.g., [Jones (1983); Munakata and Tanasawa (1990); Hintz, Schwabe and Wilke (2001); Hintz and Schwabe (2001); Schwabe (2002); Teitel, Schwabe and Gelfgat (2008); Gelfgat, Bar-Yoseph, Solan and Kowalewski (1999); Gelfgat (2011); Son and Yi (2005); Haslavsky, Miroshnichenko, Kit and Gelfgat (2011)]), and even more calculations of flow in the Czochralski configuration were carried out (see, e.g., literature review and references in [Gelfgat (2008); Szmyd, Jasczur, Ozoe and Imaishi (2008)]). However, a good comparison between experimental and numerical results remains rare. One can mention a good numerical representation of experimentally visualized steady state in [Hintz, Schwabe and Wilke (2001)], a good agreement between linear stability results of [Gelfgat (2008)] and experiments of [Munakata and Tanasawa (1990)], and agreement between the calculated and measured oscillation frequencies reported in [Munakata and Tanasawa (1990); Choi, Kim, Sung, Nakano and Koyama (1997)]. While steady flow states can be reproduced numerically with a very good accuracy, already transition to unsteadiness, which always happens beyond some critical forcing, is much more difficult to reproduce. Thus, the above mentioned good agreements [Munakata and Tanasawa (1990); Gelfgat (2008); Choi, Kim, Sung, Nakano and Koyama (1997)] were obtained for experimental fluids of a very large Prandtl number, of the order of 10^3, which does not relate directly to Czochralski grown crystalline materials. Attempts to make a comparison for more relevant experimental liquids result, as a rule, only in a qualitative agreement, e.g., [Vizman, Gräbner and Müller (2001)].

Another important issue, which is not usually addressed, is mesh independence of the results. Some relevant convergence studies for the numerical technique applied here can be found in [Gelfgat (2007)], and those performed for the Czochralski configuration in [Gelfgat (2008)]. Several results obtained for the corresponding benchmark problem [Crnogorac, Wilke, Cliffe, Gelfgat and Kit (2008)] showed that different computational approaches, when they are sufficiently accurate, do arrive to the same result. On the other hand, a successful quantitative comparison with an experiment remains a challenge.

When trying to reproduce numerically the experimental results of [Teitel, Schwabe and Gelfgat (2008); Haslavsky, Miroshnichenko, Kit and Gelfgat (2011)] we at-

tributed the disagreement either to incorrect value of surface tension temperature coefficient, or to heat losses from the free surface due to silicone oil evaporation, or to a possible contamination of a water free surface. In general, parameters of flow along the free surface are not completely known, and therefore can be a source of disagreement. To avoid this uncertainty, in the current study we covered the free surface of the Czochralski setup by a no-slip thermally insulating ring, which made the boundary conditions there definite. We expected that this will yield a better comparison between numerics and computation. However, as is shown below, there are still some disagreements between experimental and computational modeling. At low crystal rotation rates, we can qualitatively confirm the numerically observed destabilization effect, but are unable to arrive at a meaningful quantitative comparison. Only with a sufficiently strong rotation of the crystal dummy the experimental and numerical results agree quantitatively.

Seeking an explanation for the disagreement, we noticed that among geometrical imperfections of the setup, which seem to be negligible but always exist, the running water, yielding the isothermal boundary conditions, contains some small-amplitude oscillations that are caused by the thermostatic baths control system. We argued that these small-amplitude oscillations, nevertheless permanent, can trigger so-called non-modal instability of the flow, which is expected to be noticeable in subcritical flow regimes. Supplying measured oscillations of the bath water oscillations as boundary conditions, we observe non-periodic flow oscillations that attain amplitudes larger than those of the boundary conditions, and appear at the same temperature difference as is observed in the experiment. When the temperature difference exceeds the predicted linear stability limit, the oscillations become regular, and their main frequency becomes close to the one predicted by the linear stability analysis. In these regimes the frequencies of experimental and numerical oscillations are well compared, and are very close to the frequency of one of the unstable eigenmodes.

Based on the above we argue that the observed "subcritical" instabilities may appear in different experimental studies, so that their source remains undetected. Moreover, an unsteadiness introduced by an electronically controlled heating system, which is assumed to be perfectly stationary, may trigger instabilities in crystal growth and other technological processes far below the critical heating predicted by a numerical simulation.

2 Experimental setup

Our experimental setup (Fig. 1) was designed to mimic the Czochralski melt flow and is described in detail in [Haslavsky, Miroshnichenko, Kit and Gelfgat (2011)]. It consists of a precise 90 mm diameter cylindrical crucible made from transparent

Figure 1: Photo of experimental setup

glass, and a 45 mm diameter cold copper dummy imitating a crystal pulled out from the melt in a crystal growth facility. The latter plays a role of a cold rotating cover. The glass container is put inside a double-glass envelope with vacuum between its walls. Isothermal water, supplied by a computer controlled thermal bath flows between the envelope and the crucible. The double-glass envelope is closed by Teflon covers, which ensures very good thermal insulation. Assuming that thermal baths yield perfect isothermal water, and neglecting heat losses in the pipe system, we expect that after a certain time period the container wall and bottom become perfectly isothermal. The copper dummy is cooled by the cold flowing water supplied by another computer controlled thermal bath. To ensure an intensive cooling and a constant temperature on its surface, the dummy is hollow and has copper ribs inside it, so that heat transfer between the dummy's lower surface and the cold water is enhanced. The cold dummy, rotation rate can be varied in the range of 0.001-1 revolutions per second according to experimental needs. To account for possible heat losses in the pipe systems, temperatures inside the crystal dummy, and between the envelope and crucible, are measured by separate thermocouples that yield an actual temperature difference to be used in following calculations. With all the precautions made, we expect that the boundaries of our setup are isothermal to a precision supplied by the isothermal baths.

Special care is taken to match the crucible and dummy axes, as well as to align them vertically, and to make all the other surfaces perfectly vertical or perfectly horizontal. In particular, our optical table is supported by pneumatic legs making

its surface entirely horizontal. Then all the other surfaces are aligned using the table surface as a basis. Nevertheless, it is impossible to avoid small misalignments, as well as thermal asymmetries caused by the water supply system. Their effect is observed at low rotation rates as oscillations with crystal rotation frequency. A similar effect was reported in [Hintz and Schwabe (2001)]. Another possible effect of misalignment is excitation of a 2π-periodic m=1 mode, which we also observe and report below.

Temperature fluctuations are measured by very fine 0.1 mm diameter, T-type thermocouples. One pair of thermocouples is placed at the corner of the crucible, and another pair – under the crystal dummy near to the crucible bottom. The interferometry setup, seen on the photo (Fig. 1), consists of two beam splitters, two mirrors, and a beam expander that allows for a precise adjustment of the laser beams to obtain high-quality interferometry fringes on the screen. The fringes are filmed by a CCD camera.

The main uncertainty in experimental boundary conditions of a Czochralski setup is the heat balance and the thermocapillarity conditions at the free surface. The problem of heat balance can be partially resolved in a numerical model by taking into account the convection of air filling the upper part of the setup, as was done in [Teitel, Schwabe and Gelfgat (2008); Haslavsky, Miroshnichenko, Kit and Gelfgat (2011); Gelfgat A.Yu. (2008)]. However, some authors [Hintz and Schwabe (2001); Teitel, Schwabe and Gelfgat (2008)], report evaporation of experimental liquid from the free surface, which leads to an additional uncertainty since parameters of the evaporation process are not known. Another uncertainty is temperature dependence of the surface tension coefficient. For silicon oils it is usually taken from the manufacturer's supplied data (see Table 1 in [Teitel, Schwabe and Gelfgat (2008)]), which cannot be verified against independent measurements. It was shown in [Teitel, Schwabe and Gelfgat (2008)] that a small variation of the surface tension temperature dependence coefficient, or an addition of weak heat losses due to evaporation, can reduce the critical temperature difference by half. Because experiments run with the same experimental liquid for days and sometimes weeks, the free surface necessarily contaminates leading to an additional uncertainty.

To avoid the above uncertainties, in the series of experiments reported here we covered the free surface located between the crystal dummy and the container wall by a no-slip ring made from styrofoam, whose heat conductivity is very small and is about 0.033W/m$^\circ$C. To reduce the remaining heat flux from the upper ring surface the average liquid temperature in all the experiments was kept equal to the room temperature supported by air conditioning. Thus, we create perfect no-slip and heat insulation conditions, which replace the problematic conditions on the free surface. In this way we expect to fully reproduce the experimental flow in computational

Table 1: Experimentally and numerically obtained critical temperature differences and oscillation frequencies

	Experiment		Calculation		
Water					
Ω_{dummy} (rpm)	ΔT (°C)	f (Hz)	m_{cr}	ΔT_{cr} (°C)	f_{cr} (Hz)
0	0.3	0.028	0	0.84	0.034
1	0.1	0.0017	0	0.032	0.0032
4	0.1	0.0033	1	0.033	0.00033
20 cSt silicone oil					
0	1.0	0.015	1	3.65	0.046
2.5	0.5	0.0083	0	0.055	0.0018
6.8	5.0	0.013	1	0.11	0.0018
10	4.0	0.011	1	0.2	0.0020
20	0.5	0.0028	2	0.52	0.0060
20			1	0.61	0.0034
50	1.2	0.0067	3	1.08	0.0084
50			2	1.2	0.0064

modeling, and to compare quantitatively experimental and numerical results relating to the primary instability onset.

Two experimental liquids were used in the reported experiments. The first one was distilled water whose Prandtl number is $Pr\approx$6.42 at 23°C. The crucible was filled up to the aspect ratio height/radius = 1. Since the characteristic size of our setup is rather large the Grashof number is estimated as $Gr\approx$244,000ΔT, which makes the critical temperature difference smaller than 1°C. The value of ΔT is defined as the temperature difference between the heated wall and the cold dummy. A rather small difference between the hot and cold temperatures allows us to neglect temperature dependence of water thermophysical properties when computing the instability threshold. The second experimental liquid was 20cSt silicone oil whose Prandtl number is $Pr\approx$203. It was chosen because the corresponding critical Grashof number, estimated as $Gr\approx$2391ΔT, reaches its critical value at ΔT located between 3°C and 4°C. Clearly within such a small temperature difference, temperature dependence of the oil thermophysical properties can be neglected as well.

We are mainly interested in finding the threshold from a steady to an oscillatory

flow regime, as well as in studying some properties of the oscillatory supercritical states. As it already was observed in [Haslavsky, Miroshnichenko, Kit and Gelfgat (2011)] the power of frequency spectra calculated from the signals yielded by the thermocouples and the interferometer have maxima at almost the same frequencies. This is illustrated additionally in Fig. 2. Therefore, the frequency measurements are cross-validated and can be used for comparison with corresponding numerical results. Further results and comparison with the numerical results are described in Section 4.

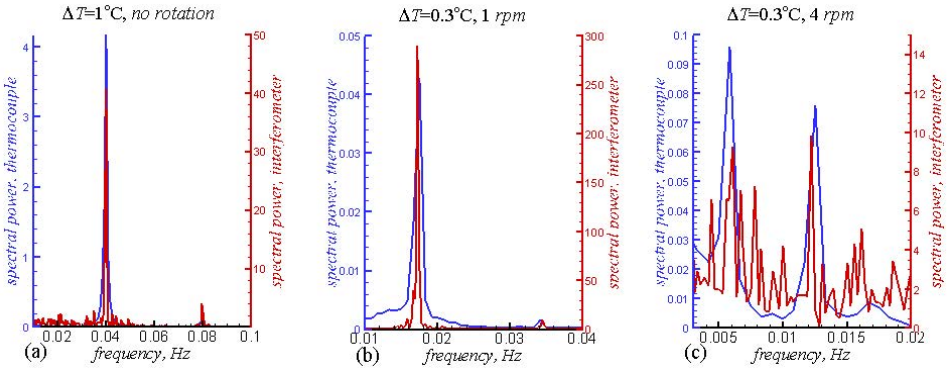

Figure 2: Comparison of the spectral power calculation from thermocouple and interferometer measurements

3 Preliminary numerical results

The problem is sketched in Fig. 3 and is formulated as follows. We consider a Boussinesq fluid in a cylindrical enclosure $0 \le r \le R_{crucible}$, $0 \le z \le H$ in cylindrical coordinates. To render equations dimensionless we introduce the scales $R_{crucible}$, $R^2_{crucible}/\nu$, $\nu/R_{crucible}$,$\rho\left(\nu/R_{crucible}\right)^2$ for length, time, velocity and pressure, respectively. The crucible radius is chosen as the characteristic length to simplify the formulation in case the dummy radius is varied. The temperature is scaled by the relation $T = \left(T^* - T^*_{cold}\right) / \left(T^*_{hot} - T^*_{cold}\right)$, where T^*_{hot} and T^*_{cold} are the maximal and minimal temperatures at the boundaries of the flow region. The set of equations for the non-dimensional velocity $\mathbf{v} = \{\mathrm{v}_r, \mathrm{v}_\theta, \mathrm{v}_z\}$, temperature T and pressure p in the domain $0 \le r \le 1$, $0 \le z \le A$ reads

$$\frac{\partial \mathbf{v}}{\partial t} + (\mathbf{v}\cdot\nabla)\,\mathbf{v} = -\nabla p + \Delta\mathbf{v} + Gr_\theta \mathbf{e}_z \tag{1}$$

$$\frac{\partial T}{\partial t} + (\mathbf{v}\cdot\nabla)\,T = \frac{1}{\mathrm{Pr}}\Delta T \quad , \tag{2}$$

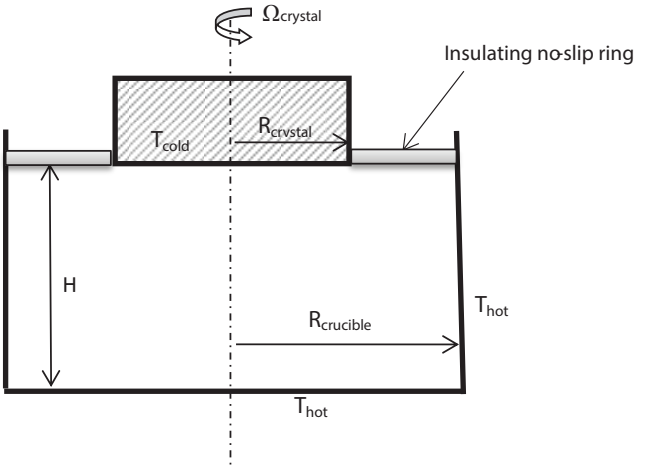

Figure 3: Sketch of the computational model

$$\nabla \cdot \mathbf{v} = 0 \tag{3}$$

Here $A = H/R_{crucible}$ is the crucible aspect ratio, $Gr = g\beta\left(T^*_{hot} - T^*_{cold}\right)R^3_{crucible}/\nu^2$ is the Grashof number, Pr=ν/χ is the Prandtl number, g is the gravity acceleration, β is the thermal expansion coefficient, and $\mathbf{e}_z$ is the unit vector in the z-direction. Three additional governing parameters are the crystal rotation Reynolds number, aspect and radii ratio, defined as $Re_{crystal} = \Omega_{crystal}R^2_{crucible}/\nu$, $A = H/R_{crucible}$ and $\eta = R_{crystal}/R_{crucible}$, respectively. The velocity boundary conditions are

$$v_r = v_z = 0 \quad \text{at} \quad z = 0,\ r = 1 \quad \text{and} \quad z = A,\ 0 \le r \le 1, \tag{4}$$

$$v_\theta = 0 \quad \text{at} \quad z = 0 \quad \text{and} \quad r = 1, \tag{5}$$

$$v_\theta = Re_{crystal}\, r \quad \text{at} \quad z = A,\ 0 \le r \le \eta, \tag{6}$$

$$v_\theta = 0 \quad \text{at} \quad z = A,\ \eta \le r \le 1. \tag{7}$$

The boundary conditions for the dimensionless temperature T are given by

$$T = 1 \quad \text{at the crucible sidewall and the bottom,} \quad z = 0 \quad \text{and} \quad r = 1; \tag{8}$$

$$T = 0 \quad \text{at the surface of the cold dummy,} \quad z = A,\ 0 \le r \le \eta; \tag{9}$$

$$\frac{\partial T}{\partial z} = 0 \quad \text{at the surface of the insulating ring,} \quad z = A,\ \eta \le r \le 1. \tag{10}$$

The thermophysical properties of water are taken at 23°C, which is the average temperature in all the experimental runs. This yields Pr=6.42, Gr=$2.44\times10^5\Delta T$, and

Re=2120Ω[*rad/s*]. Properties of the silicone oil were taken from [Rahal, Cerisier and Azuma (2007)] and its governing parameters are derived as Pr=203, Gr=2391ΔT, and Re=101Ω[*rad/s*]u

The numerical approach used here is described in detail in [Haslavsky, Miroshnichenko, Kit and Gelfgat (2011); Gelfgat (2008); Gelfgat (2007)]. The main objective of our calculations is to study stability of base axisymmetric flow with respect to three-dimensional infinitesimal perturbations. To do this we calculate axisymmetric base states and consider the three-dimensional equations linearized in the vicinity of the latter. The base flow is unstable when there exists an eigenvalue of the linearized problem with a positive real part. The eigenvalue with largest real part Λ_r is called the leading eigenvalue. The corresponding eigenvector represents the fastest growing ($\Lambda_r >0$) or slowest decaying ($\Lambda_r <0$) disturbance. The imaginary part of the leading eigenvalue Λ_i estimates the oscillation circular frequency with which the disturbance oscillates, as well as the frequency of the resulting oscillatory flow in case of oscillatory instability. We call it critical frequency. Sometimes we also interpret the imaginary parts of other eigenvalues as "frequencies" to underline that amplitude of the corresponding eigenmode grows or decays while oscillating with this frequency. Due to 2π-periodicity of the flow region in the azimuthal direction θs all the disturbances are represented as Fourier series via the complex Fourier harmonics $exp(im\theta)$. The linearized problem separates for each value of the azimuthal wavenumber m, so that the stability results are computed and reported for each integer value of m separately. Values of the Grashof number Gr_m and the temperature difference ΔT_m for which $\Lambda_r(m)$=0 are called marginal, and their minimal values over all m are called critical. The corresponding values of $\Lambda_i(m)$ yield the estimation of circular frequency with which the corresponding disturbances grow or decay. These values are called marginal frequencies, respectively to Gr_m and ΔT_m. For $m \neq 0$, the perturbation is proportional to $exp[im\theta + i\Lambda_i t]$, so that it appears as an azimuthal travelling wave, and the sign of Λ_i defines counter-clockwise ($\Lambda_i >0$) or clockwise ($\Lambda_i <0$) wave propagation. We assume that rotation of the crystal dummy is counter-clockwise. For further details the reader is referred to [Gelfgat (2008); Gelfgat (2007)] and references therein.

Results of the numerical linear stability study are shown in Figs. 4 and 5 for water and silicone oil, respectively. Frames (a) show the dependence of the marginal Grashof number (temperature difference) on the dummy rotation rate, and frames (b) – the corresponding marginal frequencies. Frames (c) and (d) zoom these results in the range of the Reynolds numbers, for which experimental measurements were carried out (see below). To make comparison with experiments easier, the results are presented both via the dimensionless parameters and experimentally defined values of Ω and ΔT. The base axisymmetric flow is stable below and on the

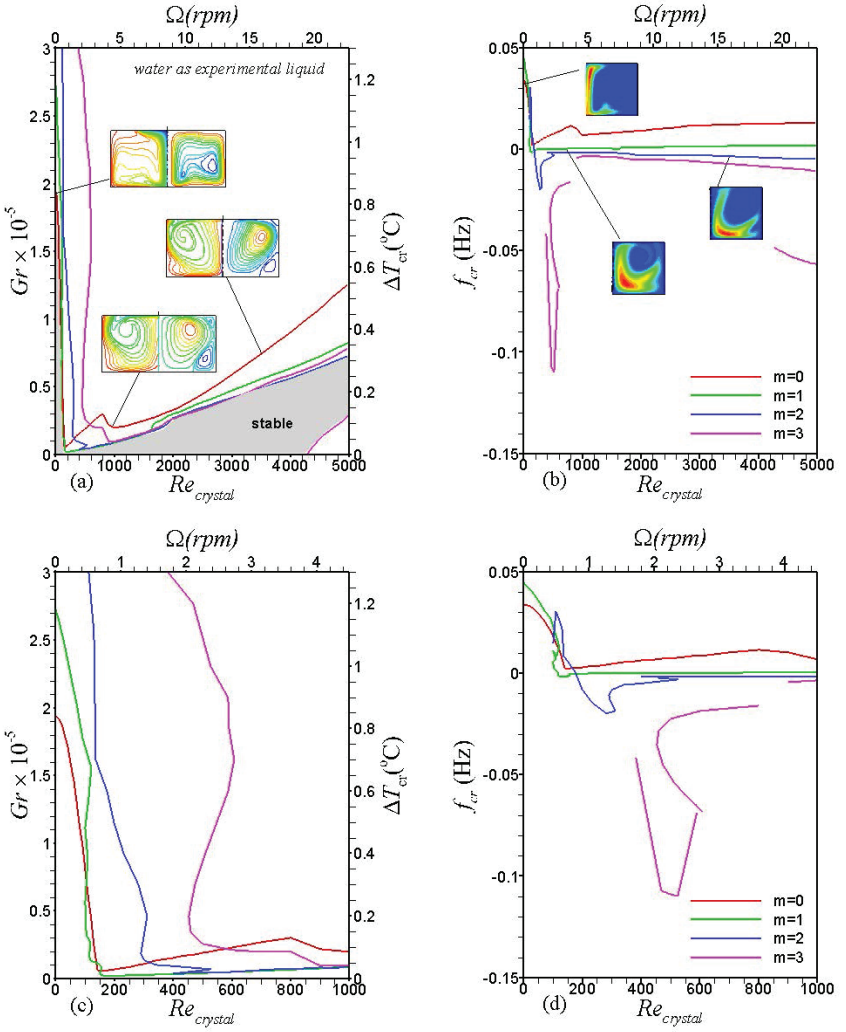

Figure 4: Results of linear stability study for water as the experimental liquid. The free surface is covered by a ring. Frames (a) and (c) - marginal stability curves; Frames (b) and (d) - perturbation frequencies in marginal points. Inserts of frame (a) show isotherms (left) and streamlines (right) of the base flows. Inserts of frame (b) show distribution of the amplitude of temperature disturbances.

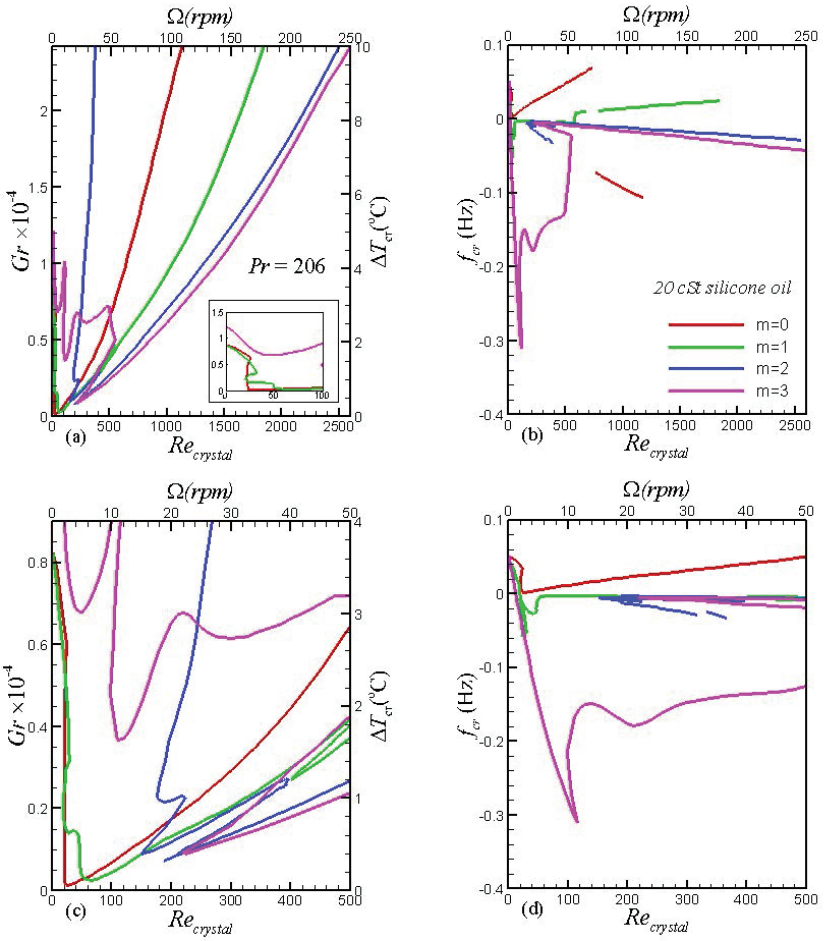

Figure 5: Results of linear stability study for 20cSt silicone oil as the experimental liquid. The free surface is covered by a ring. Frames (a) and (c) - marginal stability curves; Frames (b) and (d) - perturbation frequencies in marginal points.

left-hand side of the marginal curves. To illustrate that, a relatively small stable region is shadowed in Fig. 4a. The striking observation, however not a new one [Haslavsky, Miroshnichenko, Kit and Gelfgat (2011); Gelfgat (2008)], is a steep decrease of the critical temperature difference (the Grashof number) with a slow increase of the rotation rate. Note, that the marginal curves never reach the ΔT=0 axis, which means that the observed effect takes place due to interaction of buoyancy, centrifugal and Coriolis forces, and not by a purely rotational effect. The ex-

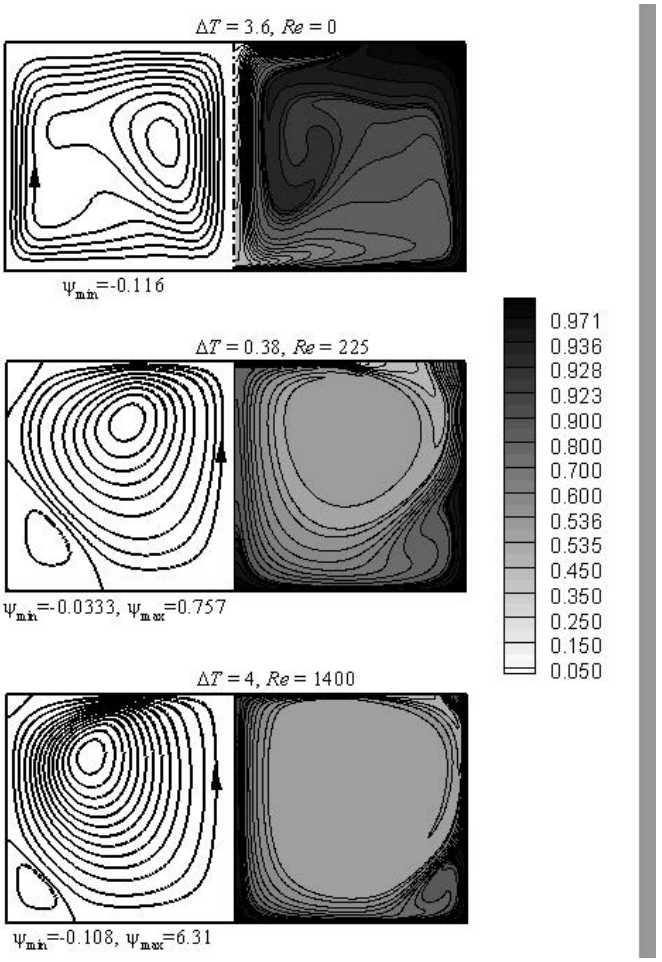

Figure 6: Streamline and isotherm patterns for 20cSt silicone oil flow. The Czochralski model with a free surface covered by a ring.

planation of this striking destabilization effect is given in [Gelfgat (2011)]. When the rotation becomes stronger the critical temperature difference slowly grows. At $Re \approx 4300$ the isothermal swirling flow becomes unstable (Fig. 4a), which gives rise to another marginal stability curve.

Examples of water flow patterns are shown in Fig.4a as inserts. In the absence of rotation the convective circulation drives the flow upwards along the crucible wall and downwards along the axis. The upper insert in Fig. 4a corresponds to this case. Two other cases illustrate flows where the centrifugal force is stronger than

the buoyancy one, so that beyond the rotating dummy the flow is driven in a radial direction from the axis to the wall. This leads to an opposite direction of the whole circulation: the flow descends along the wall and ascends along the axis. A similar change of flow pattern is observed also for silicone oil (Fig. 6). In this case, the significantly larger Prandtl number leads to a stronger convective mixing due to increase of the effective Peclet number. At large rotation rates this results in an almost isothermal core located far from the horizontal and vertical boundaries of the flow region. Note, that according to [Gelfgat (2011)], the opposite action of the buoyancy and centrifugal forces is the main reason for flow destabilization at small values of the Reynolds number (rotation rate).

Inserts of Fig. 4b show spatial distribution of the temperature disturbance amplitude, which represents, to within multiplication by a constant, the expected distribution of the amplitude of oscillatory supercritical flows. According to these patterns, as well as those reported previously in [Haslavsky, Miroshnichenko, Kit and Gelfgat (2011)], a pair of thermocouples in our experiments is installed near the bottom close to the axis. There we expect to observe relatively strong temperature oscillations, especially in the non-rotating case (see, e.g. upper insert in Fig. 4a). Another pair of thermocouples is installed in the lower corner. When the dummy rotates, as well as at large supercriticalities without the rotation, we also observe strong oscillations.

4 An attempt to compare experimental and numerical results

Measured and calculated critical temperature differences and critical frequencies are summarized in Table 1. We observe that without rotation of the crystal dummy (Ω_{dummy}=0) numerically predicted critical ΔT is noticeably larger than the one measured experimentally. In contrast, at slow rotation rates, the numerically predicted transitional values are far below the experimental ones. Only when rotation of the crystal approaches a value of 20 rpm we observe certain quantitative agreement between the experiment and computations. Some more information is gathered in Figures 7 and 8 showing the experimentally measured frequencies of flow oscillations and comparing them with those predicted by our numerical implementation of the linear stability analysis. In all the frames the black diamonds correspond to the frequencies measured at corresponding ΔT. In some of the frames we show also the value of the spectral power corresponding to a certain frequency as a number located near the diamond. The colored circles show the numerically predicted values of frequencies at the marginal values of ΔT_m corresponding to the different number of the Fourier modes m.

Since marginal and critical values obtained via the linear stability analysis correspond to oscillations with zero amplitude, one would expect that experimentally

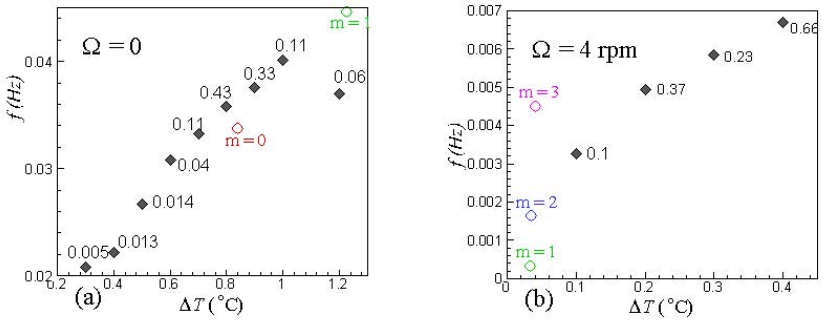

Figure 7: The Czochralski model with a free surface covered by a ring. Measured and calculated frequencies at different temperature differences for experiments with water. The black diamonds correspond to measured frequencies, the circles – to critical and marginal frequencies at the critical and marginal values of ΔT predicted by the linear stability analysis. All the colors correspond to Figs. 4 and 5.

observed transitions to unsteadiness will be detected with finite amplitude, and therefore will be slightly above the numerically predicted ones. Even in cases of subcritical bifurcations we do not expect that the depth of subcriticality is too large, so that a transition can be experimentally observed close to the numerically predicted one. For an example of such observations we mention our comparison with experiments of [Munakata and Tanasawa (1990)] reported in [Gelfgat (2008)], or a recent comparison of calculated and experimentally found transition of a lid-driven flow in a cube [Liberzon, Feldman and Gelfgat (2011)]. However, examining the non-rotating cases in Figs. 7a, 8a and Table 1 we observe that experimental transitions to an oscillatory flow takes place at significantly smaller temperature differences than those predicted numerically. A similar observation was reported in [Teitel, Schwabe and Gelfgat (2008)], however there we explained it by evaporation of the oil from the surface, and/or by a possibly incorrect value of the surface tension temperature coefficient. In the cases presented here these possibilities are excluded, however the effect remains.

An observation of the amplitudes carried by the reported frequencies yields a partial explanation of the above effect. Note that in the case of water (Fig. 7a) the spectral power of the main oscillation frequency increases by 2.5 times when ΔT is increased from 0.6 to 0.7°C, and then again increases by almost 4 times when the temperature difference is raised to ΔT =0.8°C. This steep increase of the spectral power, which estimates the oscillation amplitude, takes place close to the numerically predicted ΔT_{cr}=0.84°C. Near this value the measured and calculated frequen-

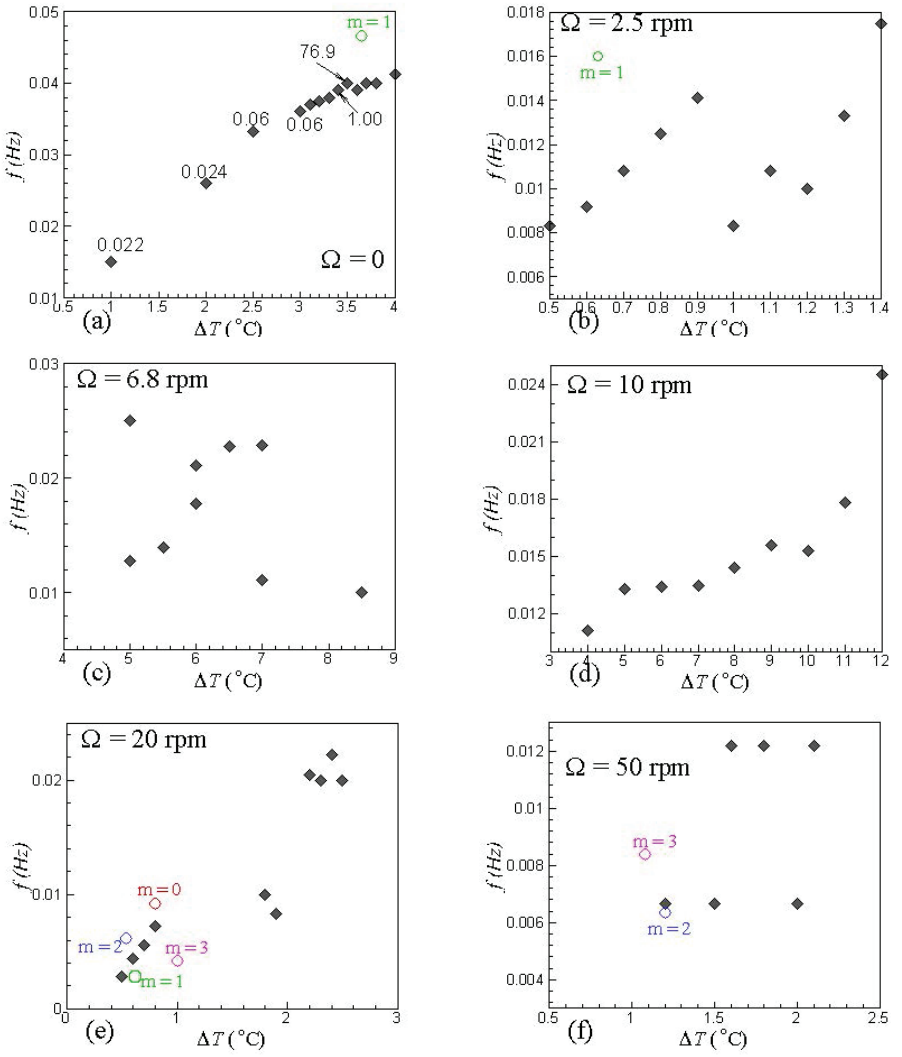

Figure 8: The Czochralski model with a free surface covered by a disk. Measured and calculated frequencies at different temperature differences for experiment with 20 cSt silicone oil. The black diamonds correspond to measured frequencies, horizontal lines – to critical and marginal frequencies predicted by the linear stability analysis. The circles correspond to the critical and marginal values of ΔT. All the colors correspond to Figs. 3 and 4.

cies also become close. A similar effect is observed also for silicone oil (Fig. 8a), where the spectral power values increases by almost 80 times, when ΔT is increased from 3.4 to 3.5°C. As mentioned below, the predicted ΔT_{cr}=3.6°C is close to this point and the predicted critical frequency f_{cr}=0.046Hz is close to the observed value of 0.04Hz. Thus, we observe that the predicted linear instability exhibits itself as a steep increase of the oscillations amplitude, which happens close to ΔT_{cr} and yields a frequency of oscillations close to the predicted f_{cr}. At the same time, the appearance of low-amplitude oscillations at lower ΔT still needs an explanation. The latter is offered in the next section.

The case shown in Fig. 7b corresponds to a moderate crystal dummy rotation of 4 rpm, which corresponds to the Reynolds number $Re\approx900$. According to Fig. 4, this value of Reynolds number corresponds to a steeply destabilized flow, for which the instability is expected to set in at ΔT_{cr}=0.03°C with the critical frequency of 3.2×10^{-4}Hz and m=1. This value of temperature difference is too low to keep it constant in the experiment, while so small frequency is almost impossible to distinguish from experimental noise. Nevertheless, the temperature oscillations, possibly appearing at larger ΔT, have such a small amplitude that they cannot be detected. Note, that the rotation affected minimal value of ΔT, at which oscillations are observed, is smaller than that without rotation (cf. Figs. 7a and 7b), which qualitatively confirms the destabilization effect predicted numerically and described in the above Section.

Experiments with a slower rotation, e.g. 1 rpm, could not successfully predict the steady – oscillatory transition. According to the numerical results, two marginal frequencies appearing at the steeply descending linear stability curves (Fig. 4) are of the order of 10^{-3} Hz. A measurement of such a slow oscillatory signal would require extremely long experimental runs with a very low noise level, since the oscillations amplitude is not expected to be large. We were unable to do it in the experiments described.

Experimental instability results with a slow rotation are more informative in the case of silicone oil. Owing to large viscosity, the numerically predicted marginal frequencies are an order of magnitude larger than those of the water, and can be measured at significantly large temperature differences, at which the oscillations amplitude becomes detectable. This is illustrated in Fig. 8b – 8e.

In the case of a very slow crystal dummy rotation of 2.5 rpm ($Re\approx26$, Fig. 8b) we detect a visible peak in the frequency spectrum starting from ΔT =0.5°C. The linear stability analysis predicts ΔT_{cr}=0.055°C with m=0 and f_{cr}=0.018 Hz (Table 1). Thus, for $\Delta T\geq$0.5°C the flow oscillations are governed by a strongly non-linear regime, which makes the frequencies incomparable with the linear stability analysis results. The next marginal mode m=1 appears to be unstable beyond ΔT_m=0.62°C

with approximately the same marginal frequency. Seemingly, this mode already does not affect the developed oscillatory flow. Here again, we experimentally observe flow destabilization by a weak crystal dummy rotation (cf. Fig. 8a and 8b), which again qualitatively agrees with the above numerical findings.

Results obtained for crystal dummy rotation of 6.8 and 10 rpm ($Re\approx$109 and 161, Fig. 8c and 8d) are similar. In both cases, mode m=1 is the most unstable. Computations predict ΔT_{cr}=0.011°C and 0.2°C with f_{cr}=0.0018 and 0.019 Hz for rotation of 6.8 and 10 rpm, respectively. A next marginal mode is m=0 with, respectively, ΔT_m=0.18°C and 0.32°C for the two above rotation rates. The difference in ΔT_m results also in the difference of the marginal frequencies, which are 0.007 and 0.012 Hz for 6.8 and 10 rpm, respectively. In the experiment we can detect visible peaks in the spectrum only starting from the temperature difference of 5°C for the rotation of 6.8 rpm and from 4°C for 10 rpm. As above, this is already a well-developed non-linear oscillatory regime, for which we cannot expect a good agreement between the measured and critical/marginal frequencies.

For crystal dummy rotation of 20 rpm ($Re\approx$210, Fig. 8e), our calculations predict that instability sets in at $\Delta T_{cr,1}$=0.55°C for mode m=2 with a frequency $f_{cr,1}$=0.006 Hz. Increasing ΔT, we observe a non-monotonic behavior of Λ_r, so that flow becomes stable at $\Delta T_{cr,2}$=0.8°C and then unstable again at $\Delta T_{cr,3}$=1.8°C (Fig. 5c). The corresponding frequencies are $f_{cr,2}$=0.009 Hz and $f_{cr,3}$=0.014 Hz (Fig. 5d). Two closest marginal modes are m=1 with ΔT_m=0.6°C and f_m=0.0034 Hz and m=0 with ΔT_m=0.8°C and f_m=0.023 Hz. In the experiment we observe oscillations of temperature starting from ΔT=0.5°C with frequency 0.0028 Hz, which increases with the increase of ΔT. This frequency is well-compared with those of the m=1 perturbation mode, which, together with the close values of ΔT_m, already can be considered as a quantitative agreement.

The case with dummy rotation of 50 rpm ($Re\approx$530, Fig. 8f) is another one, for which we observe a quantitative agreement between the experiment and numerics. The critical temperature difference here corresponds to $\Delta T_{cr,1}$=1.1°C with m=3 and $f_{cr,1}$=0.0087 Hz. This mode also exhibits a non-monotonic behavior of Λ_r and becomes stable at $\Delta T_{cr,2}$=1.9°C with $f_{cr,2}$=0.02 Hz. It finally loses stability at $\Delta T_{cr,3}$=2.4°C with $f_{cr,3}$=0.08 Hz. The two latter points are not included in Fig. 8f since the observed experimental frequencies are significantly smaller than $f_{cr,2}$ and $f_{cr,3}$. The next unstable marginal mode is m=2, whose ΔT_m=1.2°C and f_m=0.006 Hz. This is exactly the point where we start to observe the oscillations in the experiment. Other modes, m=0 and m=1 become unstable at larger ΔT and their frequencies are significantly smaller than the measured ones (Fig. 8f). We believe that in this case we do observe the instability due to a perturbation corresponding to the second azimuthal Fourier mode. Unfortunately, our visualization techniques

do not allow us to confirm that the flow pattern attains a rotational periodicity for the rotation in 180° around the axis.

5 External excitation of instability at lower temperature differences

In the following we propose an explanation to the fact that in the non-rotating case the measured critical ΔT is noticeably smaller than that predicted numerically. To address this issue, we start from an interesting observation made during the experimental measurements. Figure 9 shows temperatures measured by two thermocouples when the temperature difference was abruptly increased from 3 to 3.5°C. We observe that the temperature starts to increase almost monotonically and then suddenly produces oscillations with large amplitude. At later times the amplitude reduces, and finally the oscillations arrive to an asymptotic oscillatory state, whose amplitude is much smaller. Such a transient behavior is well-known and is described as a non-modal temporal growth of disturbances. This effect is caused by non-orthogonality of the eigenvectors of the linear stability problem. It is studied mainly for infinitely extended shear flows [Schmid (2007)], while confined flows, like the one considered here, are yet to be addressed. Nevertheless, observation of this phenomenon yields the first necessary step for the explanation we offer below.

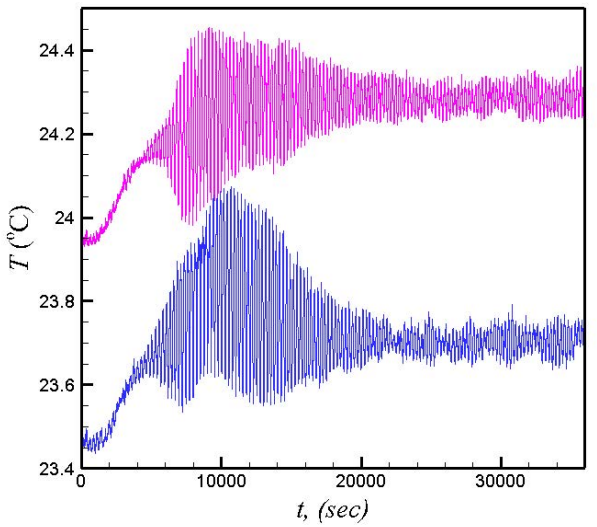

Figure 9: Temperature measured by two thermocouples after the temperature difference was suddenly increased from 3 to 3.5°C. Experiment with silicone oil.

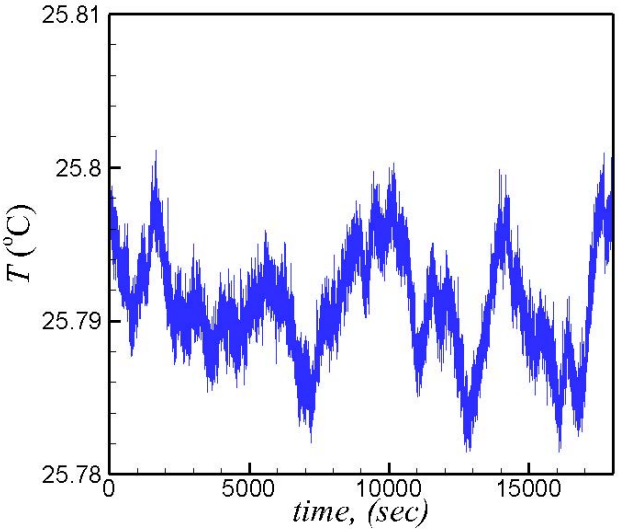

Figure 10: Temperature measured inside a thermostatic bath, which is assumed to be equal 25.8°C.

The next step is an examination of temperature inside the thermostatic bath. A measurement of the temperature inside a bath by a thermocouple reveals that the temperature there is not exactly constant, but oscillates with amplitude of approximately 0.02°C, as illustrated in Fig. 10. The periodicity of these oscillations is defined by the bath temperature controller and is not important for further discussion. At this moment we understand that the cold and hot temperatures at the boundaries are not exactly constants, but contain permanent low-amplitude oscillations.

To explain the appearance of oscillations at subcritical values of ΔT we assume that the low-amplitude oscillations of the boundary temperature values trigger non-modal perturbation growth. A non-modally growing disturbance would decay during some time, but since the boundary values oscillate permanently, they supply necessary excitation for the non-modal growth all the time. To verify this assumption entirely, one has to measure boundary temperature values, and then to perform a fully non-linear three-dimensional time-dependent calculation during a very long time, posing the measured temperatures as the boundary conditions. Such an exercise was not possible within the current study because the correct measurement of boundary temperature values was not possible, and we had no necessary computational resources to perform the mentioned 3D computations.

To make a qualitative verification of the above hypothesis, we notice that the critical instability mode in the case of water is axisymmetric (m=0). Thus, we can restrict ourselves with an axisymmetric time-dependent calculation, using for the temperature boundary conditions results of measurements in both baths. Such an exercise is affordable and simulation can be done for sufficiently long times. Having in mind the non-modal disturbances growth we expect that the oscillations we observe in the flow will have amplitudes larger than that of the boundary conditions, and frequencies of these oscillations will be comparable with the frequencies of the eigenmodes, as well as with frequencies of measured temperature oscillations.

Results of the above modeling are shown in Figs. 11 and 12. Figure 11 shows time dependence of the temperature at a point located at the axis close to the bottom, approximately at the location of one of the thermocouples. We observe irregular small-amplitude oscillations for $\Delta T \leq 0.6^{\circ}$C (Fig. 11a), while for $\Delta T \geq 0.7^{\circ}$C, the oscillations become regular and their amplitude becomes noticeably larger (Fig. 11b). Note, that the instability threshold is predicted at ΔT_{cr}=0.84°C, so that the transition from irregular to regular oscillations takes place close to the linear stability limit. Smaller amplitudes at subcritical ΔT agree with the experimental observations (Fig. 7a). The stability limit was calculated for a perfectly steady base flow, so that transition of the externally excited flow can be expected slightly earlier, as is observed. As expected, the amplitude of oscillations for $\Delta T \leq 0.6^{\circ}$C (Fig. 11a) is 2 – 3 times larger than that measured into the bath (Fig. 10), which supports our assumption about the non-modal excitation.

Figure 12 show spectral density of the time signals of Fig. 11. As expected, we observe several sharp maxima for $\Delta T < 0.6^{\circ}$C (Fig. 12a-c), which, in our opinion, correspond to different eigenmodes non-modally excited through time-dependent boundary conditions. Starting from $\Delta T = 0.6^{\circ}$C (Fig. 12d-h), a distinct most unstable mode appears and, as is shown in Fig. 13, the oscillations clearly exhibit its frequency and following harmonics that still contain some noise caused by the time-dependent boundary conditions. It is worth noting that the maximum amplitude for the time-dependent calculations (Fig. 12) was obtained at $\Delta T = 0.7^{\circ}$C, which is lower than the instability threshold $\Delta T_{cr} = 0.84^{\circ}$C. This emphasizes that in flows with possible non-normal instability, the very moderate external random forcing, e.g. time-dependent boundary conditions, can generate remarkably strong fluctuations through non-modal excitation.

To complete the above argumentation we compare measured frequencies with those obtained via the time-dependent calculations, as well as frequencies of several eigenmodes corresponding to m=0 and m=1 azimuthal wavenumbers (Fig. 13 and Table 2). Table 2 compares experimental frequencies with those obtained by the time-dependent calculations and with frequencies of leading (shown in bold) and

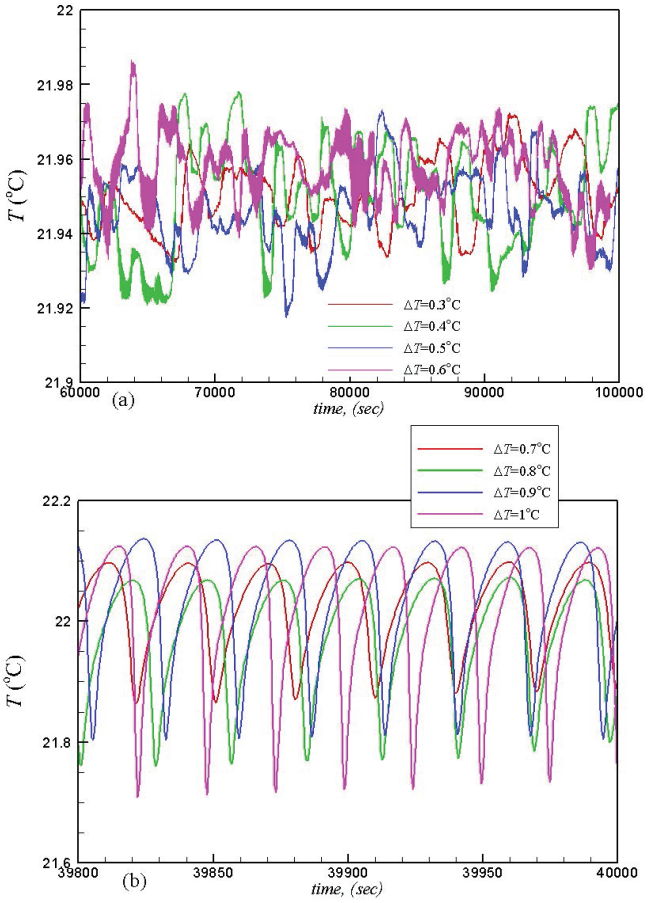

Figure 11: Histories of the calculated temperature in the location corresponding to a thermocouple positioned near the center of the bottom. The temperature boundary conditions are supplied from the measured temperatures inside the cold and hot baths.

close to leading eigenmodes. For $\Delta T \geq 0.7$°C, we observe a very good agreement between the measured and calculated frequencies, which are all located near the frequency of the most unstable axisymmetric eigenmode. At lower ΔT, the values of experimentally and calculated frequencies diverge, which can be a result of different excitation of disturbances in the experiment and calculations. Comparison of the latter values with the frequencies of the eigenmodes shows that there always exists an eigenmode corresponding to m=1, whose frequency coincides with the experimentally observed one. On the other hand, the frequencies of the cal-

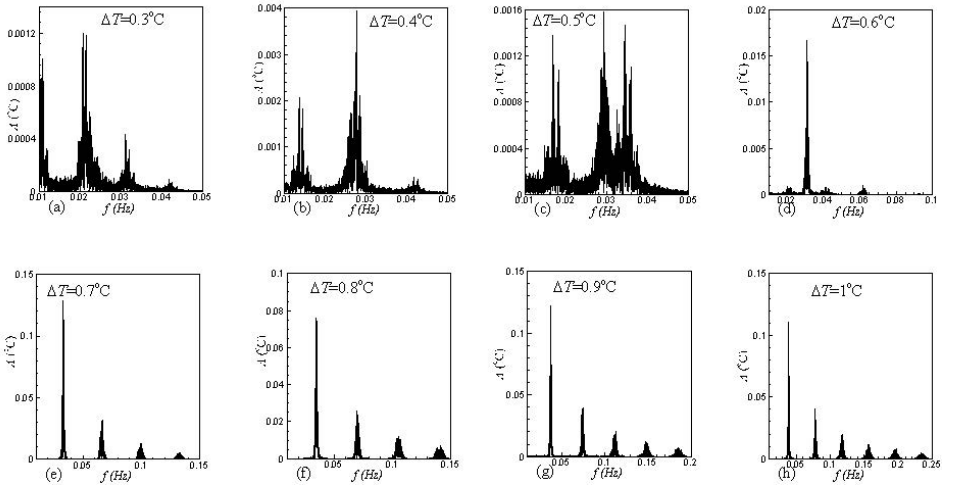

Figure 12: Frequency spectra of the temperature histories shown in Fig. 11

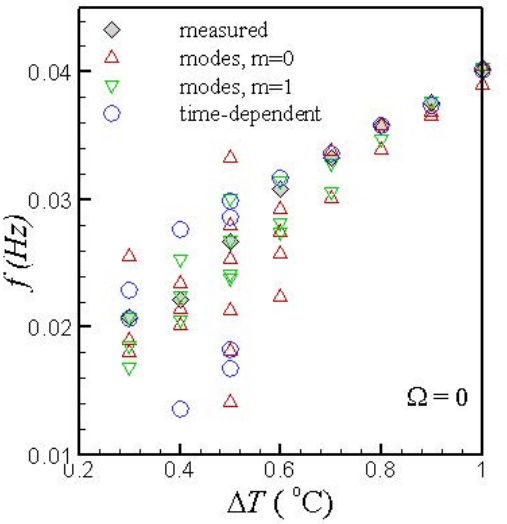

Figure 13: Experimentally measured frequencies compared with frequencies of eigenmodes whose growth rate is slightly smaller than that of the critical one, and frequencies of time-dependent axisymmetric time integration with boundary conditions incorporated from the measured bath temperatures. Experiment with water.

culated time-dependent flow depart from those of the eigenvalues, and can relate to main frequencies of the boundary conditions oscillations. Note, that the mode m=1, yielding an agreement of the measured and the eigenmode frequencies, correspond to the 2π-periodic azimuthal Fourier harmonic. This mode is most likely to be excited by an experimental setup imperfection, as is discussed above.

Table 2: Comparison of experimentally measured oscillation frequencies with the linear stability results and results of time-dependent computations implementing experimentally measured boundary conditions. Frequencies of the leading eigenmode are shown in bold.

ΔT (°C)	f (Hz) experiment	f (Hz) m=0	f (Hz) m=1	f (Hz) time integration
0.3	0.021	**0.0186**, 0.0199	0.0175	0.02286
0.4	0.022	**0.0221**, 0.0238	0.0215	0.02955
0.5	0.026	**0.0253**, 0.0293	0.0252	0.02986
0.6	0.031	**0.0284**, 0.0305	0.0286	0.03173
0.7	0.033	**0.0312**, 0.0338	0.0318	0.03361
0.8	0.036	**0.0339**, 0.0358	0.0348	0.03581
0.9	0.038	**0.0365**, 0.0369	0.0377	0.0374
1.0	0.040	**0.0390**, 0.0405	0.0404	0.0401

6 Conclusions

Experiments and calculations have been performed in a Czochralski-like flow model with a purpose to obtain reliable experimental data that can be used for validation of a computational code, especially those aimed at finding instabilities of the flow. To exclude an obvious uncertainty connected with the free surface, i.e., precise value of the surface tension temperature dependence, as well as the evaporation and contamination effects, we covered the free surface by a no-slip thermally insulating ring. The experiments were carried out for two experimental liquids: water (Pr=6.42) and 20cSt silicone oil (Pr=203).

By calculating stability diagrams for both experimental fluids, we re-obtained the effect of a sharp destabilization of flow by a slow rotation that was already reported for the Czochralski configuration in [Haslavsky, Miroshnichenko, Kit and Gelfgat (2011); Gelfgat (2008); Crnogorac, Wilke, Cliffe, Gelfgat and Kit (2008)] and was recently explained in [Gelfgat (2011)]. The present experiments carried out with a slow rotation of the crystal dummy support this prediction qualitatively, however

they were unable to measure instabilities at very small numerically predicted temperature differences, as well as to detect oscillations with the frequencies of the order 10^{-3} Hz.

Comparing the numerically predicted and experimentally measured critical temperature differences and frequencies of the appearing flow oscillations, we were able to obtain a certain quantitative agreement for the flows affected by rather strong rotation of the crystal dummy (Re>200). When rotation is slower, we observe the mentioned above destabilization, but cannot successfully compare the results. Measurements in the non-rotating case reveal that at values of temperature difference smaller than the numerically predicted critical ones some oscillations of very low amplitude emerge. At the same time, when ΔT is increased beyond the numerically predicted value, the numerically predicted frequencies corresponding to the fastest growing eigenmodes are clearly observed.

To explain the above effects, we paid attention that: (i) the flow exhibits transient growth and decay of the oscillations amplitude, which can be caused by a non-modal disturbances growth [Schmid (2007)]; and (ii) existence of small-amplitude temperature oscillations inside thermostatic baths that leads to time-dependent temperature at the crucible wall. We assumed that the experimentally observed instability can be triggered by these small-amplitude temperature oscillations at the boundaries. This assumption is supported by an additional numerical modeling, for which we imposed the measured temperature oscillations in cold and hot baths as the boundary conditions.

It is stressed that such a subcritical excitation of non-modal instability can be a case in many experiments where constant boundary temperatures are supported by an electronic feedback control system. It can be also an issue for such material processing technologies as bulk crystal growth from melt.

Acknowledgement

This study was supported by the German-Israeli Foundation, grant No. I-954 - 34.10/2007, and in part by the Israel Science Foundation (Grant 426/12) and by the Wolfson Family Charitable Trust pr/ylr/18921 & 18837.

References

Choi, J.-I.; Kim, S.; Sung, H.J.; Nakano, A.; Koyama, H.S. (1997): Transition flow modes in Czochralski configuration. *J. Cryst. Growth,* vol. 180, pp. 305-314.

Crnogorac, N.; Wilke, H.; Cliffe, K. A.; Gelfgat, A. Yu.; Kit, E. (2008): Numerical modelling of instability and supercritical oscillatory states in a Czochralski model system of oxide melts. *Cryst. Res. Technol.*, vol. 43, pp. 606-615.

Gelfgat, A. Yu.; Bar-Yoseph, P. Z., Solan, A.; Kowalewski, T. (1999): An axisymmetry-breaking instability in axially symmetric natural convection. *Int. J. Transport Phenomena*, vol. 1, pp. 173-190.

Gelfgat, A. Yu. (2007): Three-dimensional instability of axisymmetric flows: solution of benchmark problems by a low-order finite volume method. *Int. J. Numer. Meths. Fluids*, vol. 54, pp. 269-294.

Gelfgat, A. Yu. (2011): Destabilization of convection by weak rotation. *J. Fluid Mec.*, vol. 385, pp. 377-412.

Gelfgat, A. Yu. (2008): Numerical study of three-dimensional instabilities of Czochralski melt flow driven by buoyancy convection, thermocapillarity and rotation. *In: Studies of Flow Instabilities in Bulk Crystal Growth*, ed. A. Gelfgat, Transworld Research Network, 2007, pp. 57-82.

Hurle, D. T. J. (1983): Convective transport in melt growth processes. *J. Cryst. Growth*, vol. 65, pp. 124-132.

Hurle, D. T. J.; Cockayne, B. (1994): Czochralski growth. In: *Handbook of Crystal Growth* (ed. D.T.J. Hurle), Elsevier 1994, vol. 2, pp. 99-211.

Hintz, P.; Schwabe, D.; Wilke, H. (2001): Convection in Czochralski crucible. Part 1: non-rotating crystal. *J. Cryst. Growth*, vol. 222, pp. 343-355.

Hintz, P.; Schwabe, D. (2001): Convection in a Czochralski crucible: Part 2: rotating crystal. *J. Cryst. Growth,* vol. 222, pp. 356-364.

Haslavsky, V.; Miroshnichenko, E.; Kit, E.; Gelfgat, A. Yu. (2011): On experimental and numerical prediction of instabilities in Czochralski melt flow configuration. *J. Cryst. Growth,* vol. 318, pp. 156-161.

Liberzon, A.; Feldman, Yu.; Gelfgat, A. Yu. (2011): Experimental observation of the steady – oscillatory transition in a cubic lid-driven cavity. *Phys. Fluids*, vol. 23, pp. 084106.

Jones, A. D. W. (1983): An experimental model of the flow in Czochralski growth. *J. Cryst. Growth*, vol. 61, pp. 235-244.

Jones, A. D. W. (1989): Flow in a model Czochralski oxide melt. *J. Cryst. Growth*, vol. 94, pp. 421-432.

Jones, A. D. W.(1983): Spoke patterns. *J. Cryst. Growth*, vol. 63, pp. 70-76.

Kakimoto, K. (1995): Heat and mass transfer in semiconductor melts during single-crystal growth process. *Appl. Phys. Rev*., vol. 77, pp. 1827-1842.

Müller, G. (2007): Review: The Czochralski Method - where we are 90 years after Jan Czochralski's invention. *Cryst. Res. Technol.,* vol. 42, pp. 1150-1161.

Munakata, T.; Tanasawa, I. (1990): Onset of oscillatory flow in CZ growth melt.

J. Cryst. Growth, vol. 106, pp. 566-576.

Ristorcelli, J. R.; Lumley, J. L. (1992): Instabilities, transition, and turbulence in the Czochralski crystal melt. *J. Cryst. Growth*, vol. 116, pp. 447-460.

Rahal, S.; Cerisier, P.; Azuma, H. (2007): Bénard–Marangoni convection in a small circular container: influence of the Biot and Prandtl numbers on pattern dynamics and free surface deformation. *Exp. Fluids*, vol. 42, pp. 547-554.

Schmid, P. J. (2007): Nonmodal stability theory. *Ann. Rev. Fluid Mech.*, vol. 39, pp. 129-162.

Son, S.-S.; Yi, K.-W. (2005): Experimental study of the effect of crystal and crucible rotations on the thermal and velocity field in a low Prandtl number melt in a large crucible. *J. Cryst. Growth,* vol. 275, pp. e249-e257.

Schwabe, D. (2002): Buoyant-thermocapillary and pure thermocapillary convective instabilities in Czochralski systems. *J. Cryst. Growth*, vol. 237-239, pp. 1849-1853.

Szmyd, J. S.; Jasczur, M.; Ozoe, H.; Imaishi, N. (2008): Fluid flow patterns in Bridgman and Czochralski configurations. *In: Studies of Flow Instabilities in Bulk Crystal Growth*, ed. A. Gelfgat, Transworld Research Network, 2007, pp. 179-206.

Teitel, M.; Schwabe, D.; Gelfgat, A. Yu. (2008): Experimental and computational study of flow instabilities in a model of Czochralski growth. *J. Cryst. Growth*, vol. 310, pp. 1343-1348.

Vizman, D.; Gräbner, O.; Müller, G. (2001): Three-dimensional numerical simulation of thermal convection in an industrial Czochralski melt: comparison to experimental results. *J. Cryst. Growth,* vol. 233, pp. 687-698.